ACS NANO

www.acsnano.org

ARTICLE

Shape Designed Implanted Drug Delivery System for *In Situ* Hepatocellular Carcinoma Therapy

Chaochao Zhao, Qin Shi, Hu Li, Xi Cui, Yuan Xi, Yu Cao, Zhuo Xiang, Feng Li, Jinyan Sun, Jiacheng Liu, Tongqiang Li, Wei Wei, Bin Xiong,* and Zhou Li*

Cite This: https://doi.org/10.1021/acsnano.2c03768

Read Online

ACCESS | Metrics & More | Article Recommendations | Supporting Information

ABSTRACT: **In this study, an intelligent drug delivery system (DDS) based on implanted triboelectric nanogenerator (iTENG) and red blood cell (RBC) is established for *in situ* hepatocellular carcinoma (HCC) therapy. Apatinib (APA), as an oral antitumor drug, which can inhibit the expression of vascular endothelial growth factor receptor-2 (VEGFR2) is loaded inside RBC, realizing the transform from oral formulation to injection preparation. Multishape designed iTENG adapted for different implant sites and environments can harvest biomechanical energy efficiently. The electric field (EF) generated by the iTENG can increase the release of APA, and the release will decrease quickly when the EF disappears, which shows that the DDS is highly controllable. The controllable DDS demonstrates an exciting killing ability of HCC cells both *in vitro* and *in vivo* with strikingly reduced APA dosage. After implantation, the self-powered DDS has a prominent therapeutic effect of HCC-bearing rabbits, which is expected to be applied in clinical medicine.**

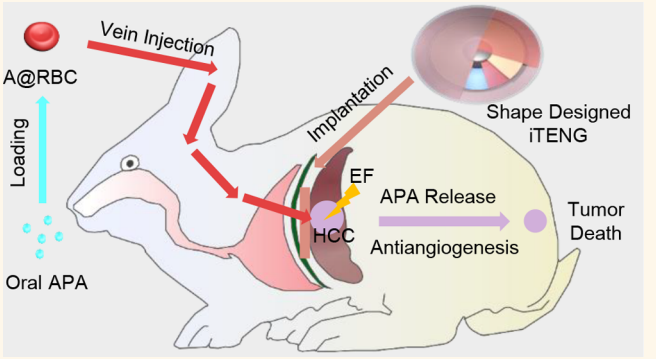

KEYWORDS: *hepatocellular carcinoma, self-powered, apatinib, triboelectric nanogenerator, drug delivery*

Hepatocellular carcinoma (HCC), as a common malignant cancer, accounts for more than 90% of primary liver cancer which is the third most frequent cause of cancer-related death.[1,2] HCC develops rapidly and seriously endangers people's health, which needs effective treatment.[3,4] Traditional cancer therapies including surgical resection, radiotherapy, interventional therapy,[5] and chemotherapy can cause serious side effects.[6] Though surgery and radiotherapy have a decent effect on patients at the very early onset, many patients miss the optimal therapeutic period, as the development course of liver cancer is not easily detected.[7] After surgery, the cancer, especially HCC, is prone to recur.[8] Interventional therapy lacks standardized treatment scheme and has no effect on lesions with the same density as normal tissue, but its targeted treatment idea is enlightening. Chemotherapy is systemic and can cause toxic reactions to organs in the whole body.[9] Precise and targeted chemotherapy, which can combine nanotechnology, has the superiority of precision and low side-effect.[10,11]

Targeted drug delivery system (DDS), as a precise and targeted chemotherapy method, can avoid the disadvantage of the chemotherapeutic drugs, such as low therapeutic efficacy and severe side effects.[12] DDS transports drugs to the place of action, and therefore vital cell destruction and side effects can be minimized. In this regard, the chemotherapeutic drugs are loaded in nanoparticles, liposomes, lipids, peptide nucleic acids, micelles, or implanted hydrogel scaffolds for cancer therapy.[13−16] These carriers can target the tumor site then release the drug, which improves the therapy effect to a great extent.[17−19] Among these, red blood cell (RBC) has been proved to be a good carrier candidate for delivering chemotherapeutic drug to tumor sites due to its no immunogenicity as autograft, perfect biocompatibility, membrane stability, flexibility, and long internal circulation time.[20,21] Drug loaded RBC can gather at the tumor due to

Received: April 18, 2022
Accepted: May 9, 2022

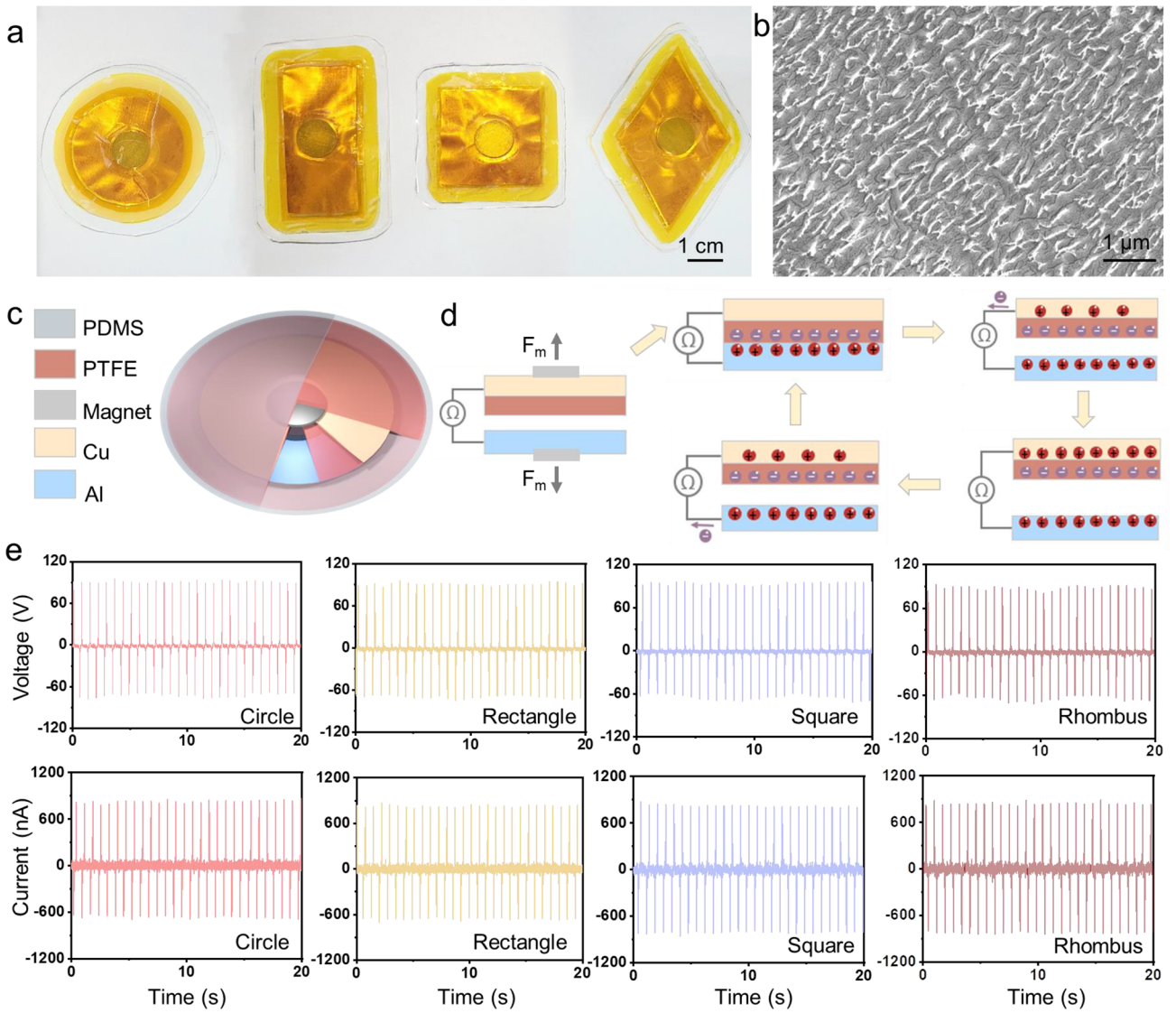

Figure 1. Structure and output performance of iTENGs. (a) Digital images of iTENGs with four different shapes. (b) Nanostructures on the PTFE surface. (c) The schematic diagram of the iTENG with circle shape. (d) Working principle of the iTENG. (e) *Voc* and *Isc* of the iTENGs with four different shapes.

the enhanced permeability and retention (EPR) effect, which is helpful for precise and targeted therapy as a carrier.

Proper drug which can be transferred by DDS affects therapeutic effect significantly. Apatinib (APA) is an oral drug for gastric and liver cancer that can highly selectively inhibit the expression of vascular endothelial growth factor receptor-2 (VEGFR2).[22] In the development and progression of tumor, VEGFR2 plays a big part through the regulation of angiogenesis, according to the analysis of pathological molecular mechanisms.[23] Hence, APA can treat HCC by reducing neovascularization. Besides, it can also kill tumor cells directly.[24,25] APA in low concentration can be injected intravenously or carried by RBC, which is an excellent drug for DDS.

Electric field (EF) has proven to have an influence on the molecule transmission of the RBC.[26,27] EF is regarded as an attractive choice for an RBC-based DDS control system due to its noninvasiveness, easy manipulation, low cost, and the ability to reach target tissues.[28] Traditional commercial EF sources are usually enormous and insecure, which prevent their applications in portable, wearable, or implantable devices.[29] Especially for implanted EF based DDS, energy depletion is a serious problem to be solved.[30,31] TENG can be a promising solution due to its infinite energy supply and small scale.[32−34] In this regard, our previous work developed a DDS using a self-powered triboelectric nanogenerator (TENG) to control the doxorubicin (DOX) release from DOX loaded RBC, which demonstrated an excellent therapy efficacy of cervical cancer.[35] Unfortunately, the prepared TENG was not implanted into live animals because the implant sites and environments were complicated. The implanted TENG (iTENG) should be well matched with the inner tissues including shape, size, elastic strength, flexibility, and output performance.[36]

In this work, we demonstrated an implanted DDS based on shape designed iTENG and RBC for *in situ* HCC therapy. The DDS was developed to precisely control the chemotherapeutic drug release from the APA loaded RBC (A@RBC). The encapsulated iTENGs suitable for different implant sites and environments were fabricated. The self-powered DDS not only had excellent killing ability of HCC cells *in vitro*, but also

https://doi.org/10.1021/acsnano.2c03768
ACS Nano XXXX, XXX, XXX−XXX

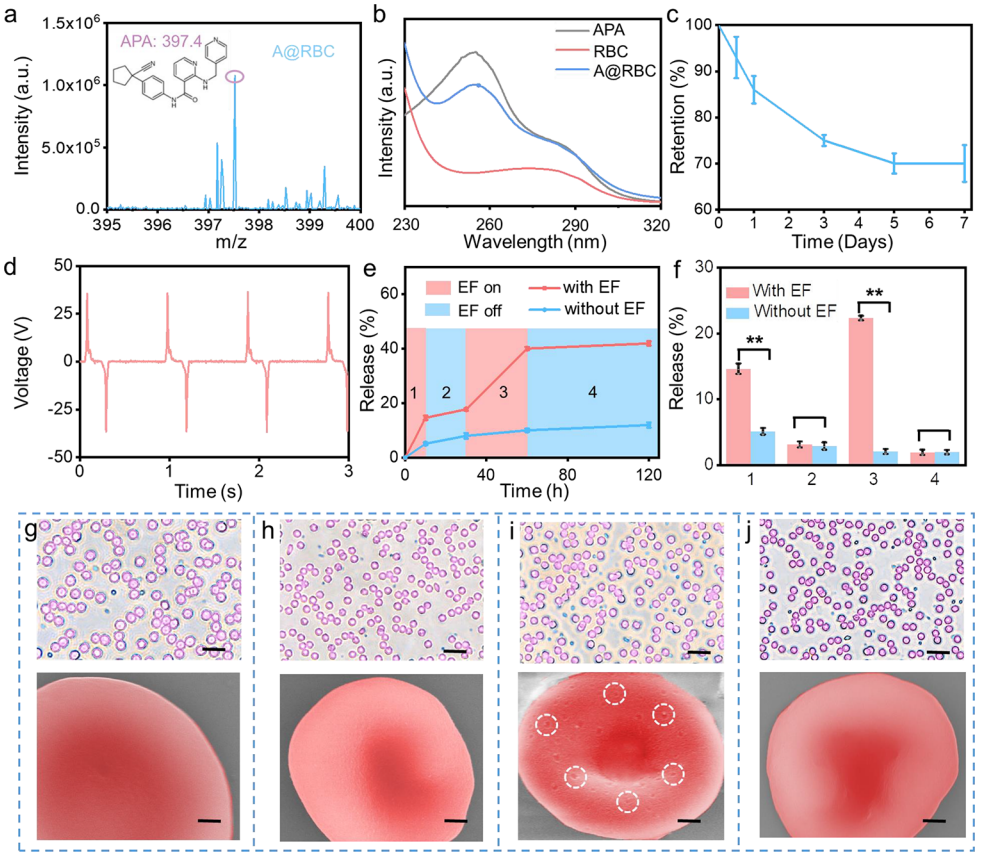

Figure 2. Controlled release of APA from A@RBC. (a) The mass spectrum of A@RBC. (b) The UV−vis spectrum of APA, RBC, and A@RBC. (c) The self-release of APA from A@RBC. (d) The voltage between two adjacent electrodes after the A@RBC was seeded. (e,f) Kinetics of the iTENG-controlled drug release. The EF enhanced APA release in a controllable mode. $^{**}p < 0.01$, $^{*}p < 0.05$. g-h) The optical microscope (the upside, scale bar: 10 μm) and pseudocolored SEM images (the downside, scale bar: 200 nm) of innate RBC, A@RBC, A@RBC+EF, and A@RBC after EF.

inhibited tumor growth in the subcutaneous tumor bearing mice. In further, the self-powered DDS was implanted between the diaphragm and liver of rabbits and demonstrated an outstanding *in situ* antitumor efficacy.

RESULTS AND DISCUSSION

Fabrication and Characteristics of the iTENG. For implant application, the shape of iTENG should be adapted for specific implant site and environment. In this experiment, iTENGs with four different shapes (circle, rectangle, square, and rhombus) were prepared, as shown in Figure 1a. Taking the iTENG of circle shape as an example, the detailed structure is illustrated in Figure 1c. The two friction layers were aluminum (Al) foil and polytetrafluoro ethylene (PTFE) membrane, respectively. Nanostructures on the PTFE surface was produced by inductively coupled plasma (ICP) etch to improve the output of the iTENG (Figure 1b). A cuprum (Cu) electrode with a thickness of about 200 nm was magnetron sputtered on the surface of the PTFE membrane. Two tiny magnets with about 8 mm in diameter were sticked to the surface of the Cu electrode and Al foil to separate them via magnetic repulsion. The magnet structure which potently guaranteed the separation and contact process of iTENG worked better than previous spacer or keel structure especially in circle shape. Based on this structure, iTENGs with irregular shapes such as arc shape and star shape would also working normally. The TENGs were packaged by kapton tape, PTFE tape, and polydimethylsiloxane (PDMS) to protect the iTENG from liquid environment. Based on the coupling of contact electrification and electrostatic induction, the detailed working principle of the TENG is illustrated in Figure 1d. Under periodic contact and separation of two triboelectric layers, electrons were driven back and forth through the external circuit. After encapsulation, the iTENGs of four different shapes could similarly reach the open-circuit voltage (*Voc*) of 90 V, short-circuit current (*Isc*) of 850 nA (Figure 1e) and transferred charge (*Qsc*) of 35 nC (SI Figure S1) when the friction areas were 9 cm^2, which suggested that our iTENGs were proper to serve as implanted power source for DDSs.

APA Loading and Controlled Release by iTENG. The APA was encapsulated into RBC based on the classical hypotonic dialysis method. First, fresh RBC was swelling in hypotonic solution containing the chemotherapeutic drug APA, during which adenosine triphosphate (ATP), glutathione (GSH), some other metabolic stabilizers, and low temperature were provided to protect the RBC from oxidative damage. Besides, the pH was strictly controlled between 5 and 6, for the membrane structure could be destroyed by low pH (SI Figure S2). After incubated with hypotonic solution for 40 min, the inflated RBC were transferred into a hypertonic buffer (300 osm) to obtain the APA loaded RBC (A@RBC). The molecular mass of 397.4 was detected in both APA (SI Figure S3) and A@RBC samples (Figure 2a), suggesting that APA had been successfully loaded into the RBC. The UV−vis

https://doi.org/10.1021/acsnano.2c03768
ACS Nano XXXX, XXX, XXX−XXX

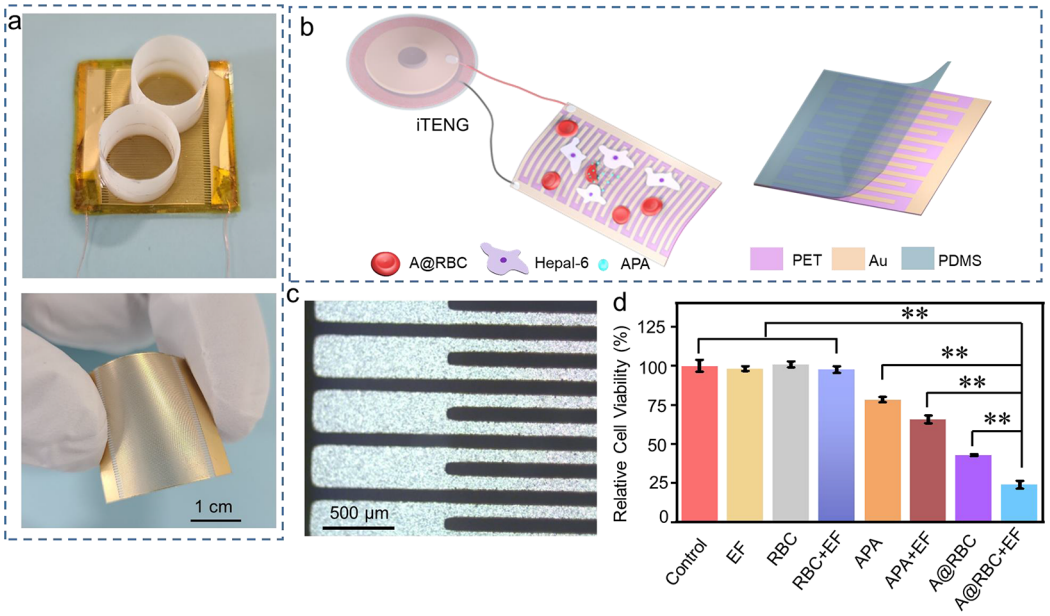

Figure 3. Self-powered EF device to treat hepal-6 cells. (a) Digital images of the EF stimulation device and the flexible interdigitated electrode. (b) The schematic diagram of self-powered EF DDS to treat Hepal-6 cells. (c) Optical image of the interdigitated electrode. (d) The cell viabilities in the control, EF, RBC, and RBC+EF group had little difference. The cell viabilities in the APA, APA+EF, A@RBC, and A@RBC+EF group decreased obviously. The data was based on the mean ± SD and error bars were based on at least three samples. $^{**}p < 0.01$, $^{*}p < 0.05$.

spectra further confirmed that the A@RBC had the same emission peak as APA at 254 nm, while the control RBC did not have obvious absorption peak (Figure 2b). From the standard curve quantified by UV−vis spectra (SI Figure S4), it was calculated that about 177 μg APA molecules were encapsulated into 1 mL RBC membrane. As for self-release behavior, above 70% of APA was maintained in the RBC membrane after a week, showing a relatively low intrinsic APA release (Figure 2c).

The same two-dimension (2D) stimulation device as previous work was used for the drug release *in vitro*.[35] We investigated the voltages of 0 V, 5 V, 15 V, 30 V, 90 V, and 180 V on the APA release from A@RBC. The release rate of APA was slightly increased as the voltages were 5 and 15 V. When the voltage was above 30 V, APA release rate was obviously accelerated, and the release rate was increasing with the rising of voltage (SI Figure S5). After the A@RBC sample was seeded in the device, the voltage between two adjacent electrodes could reach 32 V (Figure 2d). As shown in Figure 2e, the group with EF stimulation showed much more APA release than that without EF during the Period 1 of the first 10 min. Once the iTENG stopped working, the release rate of EF group quickly slowed down in the Period 2 of the next 20 min. Then stimulation had been performed for 30 min in Period 3, during which the release of the stimulation group had reached 40%, much faster than that of the control group (about 10%). Next when the EF disappeared again, the release rate of the stimulation group was down to the baseline in Period 4. Figure 2f showed that after stimulation for 10 min, the released APA was about 3 folds of the control group; during Period 3, the released amount of the EF group was about 11 folds of the control. As the iTENG ceased work, the group with EF did not show any difference of APA release from the group without EF during Period 2 and Period 4. We continuously stimulated the A@RBC for 24 h with the voltage of 32 V, and the maximum release of APA was about 71.5% (SI Figure S6). These results demonstrated that the EF generated by iTENG could accelerate the release of APA in a controllable mode.

To further observe the structure changes of the membranes, optical microscope and scanning electron microscope (SEM) were used in the next experiment. The original RBC (Figure 2g) and A@RBC (Figure 2h) exhibited normal structure, while the diameter of the A@RBC became much smaller, mainly because a great deal of inside hemoglobin escaped during the hypotonic progress. After EF stimulation for 10 min, some RBC exhibited nanopores on the surface of RBC (Figure 2i). This result showed that electroporation of A@RBC was triggered by the EF. After the EF was revoked, the membranes were self-healing and the pores disappeared (Figure 2j). Under the highfield provided by iTENG, nanopores were generated on the RBC membrane. After the EF disappeared, the pores were self-healed, showing a controllable release pattern by the electroporation mechanism. After stimulation for 3 days with the voltage of 180 V, the SEM picture showed that most A@RBCs were still intact (SI Figure S7).

iTENG Controlled EF DDS to Treat Hepal-6 Cells. The self-powered EF stimulation device was integrated with an iTENG and an interdigitated electrode. The substrate was polyethylene terephthalate (PET), so the stimulator could be flexible, as shown in Figure 3a. The PET substrate was deposited by Au electrodes with gaps of 100 μm and widths of 100 μm to increase the EF applied on the A@RBC (Figure 3b,c). Further, the surface of Au electrodes was covered by an ultrathin PDMS film for insulation. When the cells were seeded in the hollow cylinders that fixed on the PDMS surface, they could be stimulated by the EF generated by the iTENG. After incubation with APA, RBC, or A@RBC for 1 h, the hepal-6 cells were stimulated by the EF for another 1 h and further cultured for 24 h without EF. Then the cell viability was evaluated by cell counting kit-8 (CCK-8) assay. The results showed that EF stimulation and RBC did not have any difference on the cell state. The viability of Hepal-6 cells in 1

https://doi.org/10.1021/acsnano.2c03768
ACS Nano XXXX, XXX, XXX−XXX

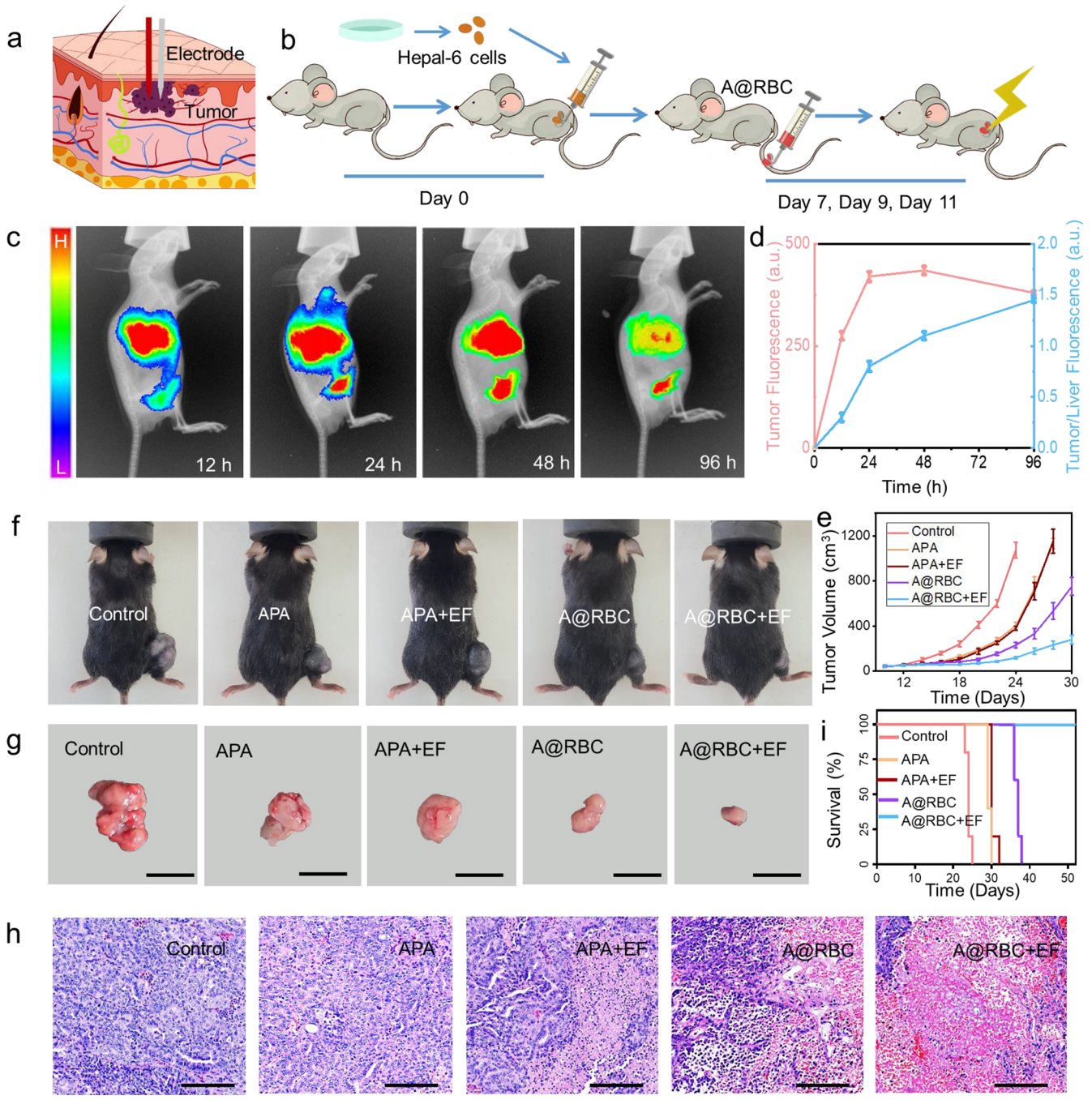

Figure 4. Controlled EF DDS to treat the subcutaneous tumors of 60 mice. (a) The sketch map of microneedle electrodes to delivery EF to the tumor. (b) The schematic illustration of the experiment design. (c) The tumor accumulation of A@RBC measured by *in vivo* animal imaging system at 12 h, 24 h, 48 h, and 96 h. (d) The accumulated A@RBC in tumor and the ratio of tumor-to liver fluorescence intensity. (e) The tumor growth curve *in vivo*. (f) The digital pictures of the mice on Day 30. (g) Image of the isolated tumors in each group on Day 30. Scale bar: 1 cm. (h) The HE immunohistochemistry images of the tumors in each group. Scale bar: 100 μm. (i) The survival curve of mice from different treatment groups.

μg/mL APA decreased to 78.4%, while the cells in free APA combined with EF group (APA+EF) had a slightly lower viability to 65.7%, mainly because the EF increased the cell endocytosis of APA. The cell viability in A@RBC group decreased to 42.8%, for the colocation of A@RBC and hepal-6 cells promoted the hepal-6 cells to uptake more of the released APA. When combined with EF, the cell viability decreased to 23.9% in the A@RBC + EF group, which suggested that the self-powered EF DDS had enhanced the ability of killing liver cancer cells (Figure 3d).

iTENG Controlled EF DDS to Treat Subcutaneous Tumor in Mice. For the subcutaneous liver cancer model, 60 Hepal-6-tumor bearing c57 mice were constructed and a pair of steel microneedles were utilized to delivery EF provided by the iTENG to the tumor site (Figure 4a). The experiment design was illustrated in Figure 4b. Hepal-6 cells were seeded subcutaneously at the back leg on day 0, then PBS, APA, or A@RBC was injected through tail vein when the tumor volume grew to 100 mm^3. Besides, the accumulation of the A@RBC after injection was also monitored by the *in vivo* animal

https://doi.org/10.1021/acsnano.2c03768
ACS Nano XXXX, XXX, XXX−XXX

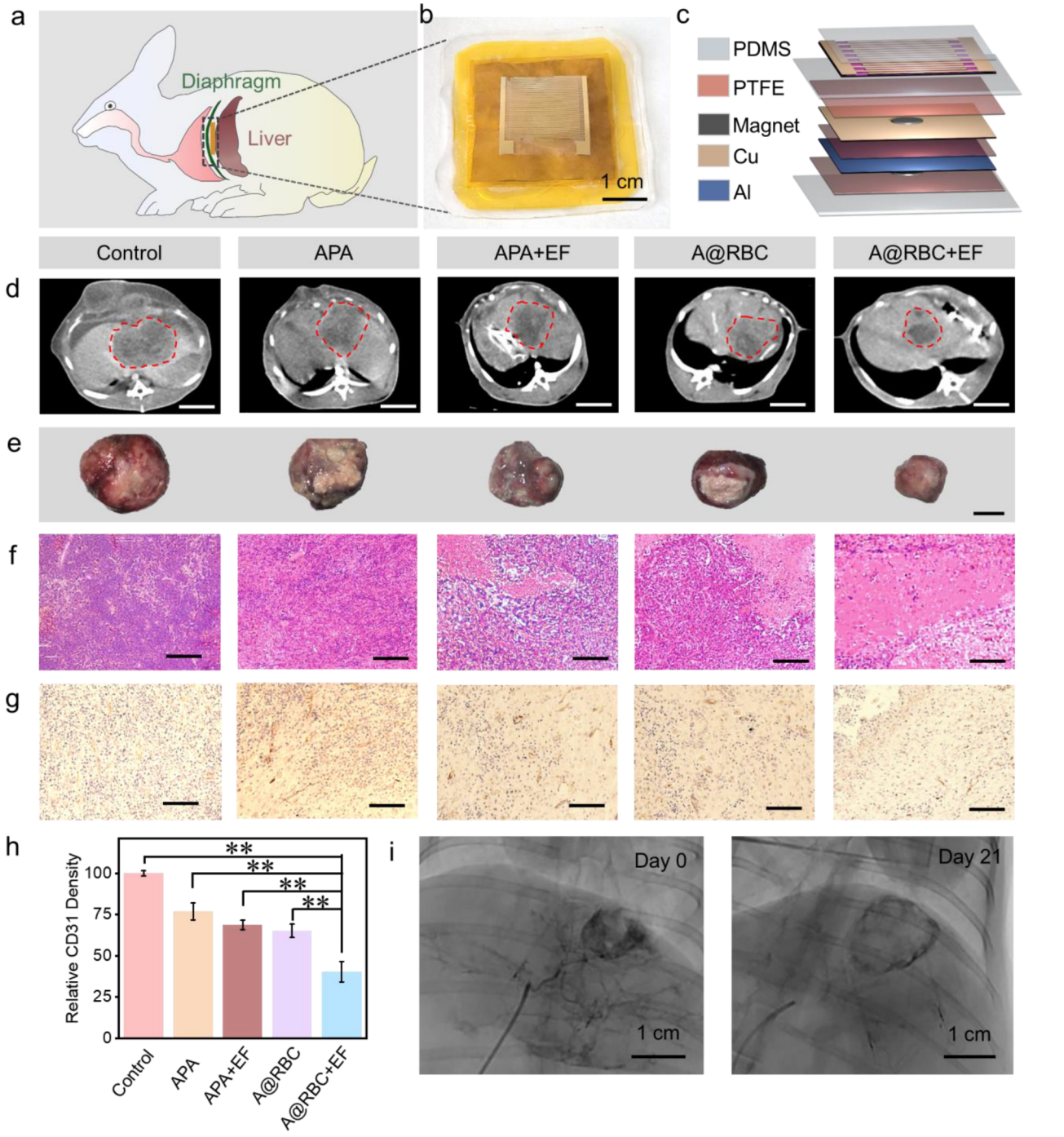

Figure 5. ITENG controlled implanted DDS to treat *in situ* tumor of rabbit. (a) Schematic diagram of the iTENG based devices implanted between the tumor and diaphragm to provide EF. (b) Digital image and (c) schematic diagram of the iTENG connected with interdigitated electrodes. (d) The enhanced CT scan of tumors in each group on Day 21. Scale bar: 1 cm. (e) Image of the isolated tumors in each group on Day 30. Scale bar: 1 cm. (f) The HE immunohistochemistry images of the tumors in each group. Scale bar: 100 μm. (g) The CD31 immunohistochemical staining of neovascularization in all groups. Scale bar: 100 μm. (h) The relative CD31 density in each group. ** $p < 0.01$, * $p < 0.05$. (i) The DSA of a rabbit in A@RBC group on Day 0 and Day 21.

imaging system. At 12 h after injection, some of the A@RBC reached the tumor site, while most accumulated in the liver. From 24 to 48 h after injection, the amount of A@RBC at the tumor site kept increasing rapidly and at 48 h the fluorescent density of the tumor was nearly equivalent to that of the liver. The fluorescence images of all major organs compared to tumors for control and treated animals at 72 h confirmed that the A@RBC could reach and gather at the tumor site (SI Figure S8). Then at 96 h after inoculation, the cumulative A@RBC in the liver decreased hastily while most A@RBC remained at the tumor site due to the EPR effect of tumor (Figure 4c). Figure 4d showed the change of tumor fluorescence intensity and the time-varying intensity ratio of tumor-to-liver. To value the therapeutic efficiency, the mice with tumor were separated in control (PBS), APA, APA+EF, A@RBC, and @RBC+EF groups randomly. The APA dose of

https://doi.org/10.1021/acsnano.2c03768
ACS Nano XXXX, XXX, XXX−XXX

5 mg/kg body weight in the APA, APA+EF, A@RBC, or A@RBC+EF group was administrated three times on Day 7, Day 9, and Day 11, respectively. In the PBS group, the tumor grew up in an uncontrollable pattern. APA or APA+EF could slightly inhibit the growth of the liver tumor but could not eliminate it. Due to the accumulation of A@RBC in the tumor, the growth speed of tumors significantly slowed down. In the meantime, combined with EF stimulation, A@RBC+EF group could effectively enhance the suppressive effects on tumor progress. The tumors barely grew before Day 22 and began to grow slowly after that time (Figure 4e). On Day 30, the mice could hardly bare the tumor in control group, while the tumor in A@RBC+EF group was the smallest (Figure 4f). Half of the mice were euthanized, and the tumors in each group were stripped out. In A@RBC+EF group the tumors had much smaller volume than that in the other groups, as shown in Figure 4g and SI Figure S9. Meanwhile, hematoxylin-eosin (HE) immunohistochemistry staining (Figure 4h) and Ki67 experiment (SI Figure S10) also demonstrated the minimal tumor cell proliferation in the A@RBC+EF group. The survival time of mice in A@RBC+EF group was significantly extended, and no individual death happened during the observation period (Figure 4i). The body weight of the mice was recording every 2 days and kept stable during the treatment period, suggesting negligible harm caused to the mice (SI Figure S11). Above results suggested the exciting therapeutic efficacy of the self-powered DDS in mice.

iTENG Controlled RBC DDS to Treat *In Situ* Tumor of Rabbit. Next, the antitumor efficiency and antiangiogenic activity of the iTENG controlled A@RBC DDS was studied *in situ* live tumor of rabbit (Figure 5a). Before this, we implanted the iTENGs subcutaneously in rats for 1, 2, and 3 months to test the biocompatibility and stability of the self-powered EF devices. The HE staining and Masson's trichrome staining of the tissue slices retrieved at 1, 2, and 3 months showed that the host immune responses were minimal (SI Figure S12). Besides, the flow analysis of the implant sites was investigated, which had little host innate immune macrophages (SI Figure S13, brilliant violet (BV)-labeled F4/80) and neutrophils (SI Figure S14, APC-labeled Ly6G) at the formed tissues around the implants, indicating negligible inflammation. Also, the voltage outputs of these self-powered EF devices kept stable after 3 months of implantation, demonstrating favorable stability (SI Figure S15). A square-shaped iTENG was connected to a pair of perylene C packaged microneedle electrodes and flexible PDMS encapsulated interdigitated electrodes to increase the contact chance of tumor vessels and electrodes in the experiment (Figure 5b and Figure 5c). After the iTENG was implanted between the tumor and diaphragm of a rabbit (SI Figure S16), it could generate a voltage of about 33 V (SI Figure S17). The rabbits were randomly divided into control, APA, APA+EF, A@RBC, and A@RBC groups when the diameter of tumors reached about 1 cm (Day 0). In addition, the enhanced computed tomography (CT) scan of tumor in each group was performed on Day 7 (SI Figure S18, the upside) and Day 21 (Figure 5d). The tumors grew rapidly, and ascites appeared around the liver in the control group, which indicated the tumors deteriorated seriously. With APA injected, it could induce a handful of necrosis on some tumors but could not control the tumor growth. Similar to the experiment results of mice, A@RBC+EF group achieved the most effective antitumor performance in the VX2 tumor bearing rabbits. The same tumor-bearing rabbits in each group were sacrificed on Day 7 and Day 21, and the picture of tumor specimens were shown in SI Figure S18 (the downside) and Figure 5e, respectively. The tumor volumes in A@RBC+EF group were smallest among all the groups. HE immunohistochemistry staining further confirmed that the A@RBC+EF group had the maximum tumor necrosis compared with the other groups (Figure 5f). The Ki67 experiment also indicated the minimal tumor cell proliferation in the A@RBC+EF group (SI Figure S19). The CD31 immunohistochemical staining of neovascularization is shown in Figure 5g. Taking the control group as a baseline, the neovascularization decreased relatively in the APA, APA+EF and A@RBC groups but no significant difference was found. Interestingly, the A@RBC+EF group had less angiogenesis compared with the other groups (Figure 5h). In addition, in A@RBC+EF group more tumor vessels could be clearly observed by digital subtraction angiography (DSA) immediately after the iTENG implantation on Day 0. While on Day 21, the tumor vessels decreased obviously (Figure 5i), which indicated that the iTENG controlled DDS could highly inhibit the tumor growth by reducing angiogenesis. These results demonstrated that the self-powered implanted DDS was a feasible method for HCC therapy.

CONCLUSIONS

HCC, a common malignant cancer, is a serious threat to human health. Among the cancer clinical treatments, chemotherapy is widely used, but usually does harm to the heart, intestines, stomach, kidney, and so on. In this regards, targeted DDSs are developed to circumvent these side effects, which can directly reach and penetrate into the tumors. They significantly reduce drug dose compared with the oral method, which can reduce the damage to vital cells and tissues markedly and minimize harm to normal organs.[37,38] APA is usually administrated orally, but the induced complications such as hypertension, proteinuria, and hand-foot syndrome limit the continual use of the drug.[39,40] The oral dose is 10−20 times higher than intravenous injection, thus causing strong drug resistance.[41−43] In this regard, the APA is loaded in nanoparticles, liposomes, lipids, peptide nucleic acids, or micelles to realize intravenous injection in most recent works.[44,45] In these noninvasive systems, the structures of the carriers are disrupted by the acidic and anaerobic tumor microenvironment to passively release drugs in a relatively short time, which cannot control the drug release rate strictly. Other implants, such as hydrogels and scaffolds, can control the drug release by infrared light or the tumor microenvironment.[13,17−19] In addition, the hydrogel scaffolds can also help with tissue reparation especially in breast cancer.[15,16] However, the nonspecific hydrogel systems are characterized by low drug loading ability, unwanted drug leakage, limited biocompatibility, and severe drug resistance. Moreover, the sophisticated hydrogels with light-responsive-drug-release and functional agents increase the preparation process and the complexity of DDS. For our implantation system, the small device size, the tunable device shape for different implant sites, and the advanced surgical technique can also realize minimal invasion. Moreover, for the patients who require both surgical treatment and chemotherapy, the implantation process can be accomplished during surgery. However, for the patients who cannot afford major surgery, the implantation of microelectrodes alone to the tumor site is an optimal choice. The self-powered DDS can precisely and efficiently control the release rate of APA according to the willingness of the individual or the doctor for

https://doi.org/10.1021/acsnano.2c03768
ACS Nano XXXX, XXX, XXX−XXX

a longer time. Besides, the drug release responding to EF is very quick. What's more, the EF generated by the TENG can also enhance the endocytosis of tumor cells to chemotherapeutical drug, thus further reducing the drug dose and side effect.[46] APA has the approximate molecular weight with DOX, which can be loaded by RBC similarly. As an oral formulation for HCC therapy, APA can be transferred into injection dosage by RBC loading.

In this work, we developed iTENGs with different shapes for EF controlled DDS, which suited for implantation in different sites and environments. The magnets in iTENG were the key to potently guarantee the detach and contact process, which improved the output of iTENG significantly. The EF provided by the iTENG was demonstrated to effectively increase the APA release from RBC by electroporation mechanism. APA could potently inhibit HCC cells proliferation and tumor growth both in subcutaneous liver tumor and *in situ* liver tumor by reducing neovascularization.

To research the performance of iTENGs *in vivo*, the iTENGs were implanted between the diaphragm and liver to harvest mechanical energy from the body breath. With iTENG acting as the electric source and the microneedles and flexible interdigitated electrodes serving as the electrodes, the integrated DDS could be entirely implanted into the body to provide EF for intrabody tumor therapy. With reduced drug dosage of 5 mg/kg body weight, this self-powered system remained great antitumor efficiency. In this regard, our iTENG-based EF DDS is very promising to be applied in implantable medicine.

In summary, we successfully established a self-powered controllable DDS for *in situ* HCC therapy. The iTENGs with different shapes were fabricated for implantation in different sites and environments. The self-powered DDS demonstrated a controllable release mode. The EF stimulation provided by the iTENG increased the APA release from A@RBC, while after the EF was withdrawn, the enhanced release would also cease. The iTENG could generate EF to increase APA release for *in situ* HCC therapy. These results demonstrated a distinguished therapeutic effect of cancer with very low APA dosage by the self-powered controllable DDS. This implanted DDS is highly promising to be used in the clinical medicine.

EXPERIMENTAL SECTION

Fabrication of the iTENG. The contact-separation mode iTENG designed for this experiment had a PTFE membrane with surface microstructures to serve as one triboelectric layer, and an alumimum (Al) sheet as the other triboelectric layer and electrode. The inductively coupled plasma (ICP) reactive ion etching process was executed on the PTFE surface, in order to achieve nanostructures. The detailed parameters for the ICP treatment could be seen in the reference paper.[35] A Cu film was magnetron sputtered on the PTFE membrane to serve as an electrode with a thickness of about 200 nm. To separate the two triboelectric layers, a pair of magnets were pasted on their back surface. Then the nude iTENG was in sequence packaged by Kapton tape, PTFE tape, and PDMS. The output of iTENG was measured by Keithley 6517 electrometer and tektronix oscilloscope system.

Preparation of A@RBC. APA was dissolved in HCl solution (1 M) and then the pH of mixed solution was adjusted between 5 and 6. The RBC were derived from the whole blood that acquired from c57 mice by centrifugation (2500 rpm, 10 min). After washing with 1× PBS, the sedimentary RBC was suspended in the PBS which was 30% in volume. Hypotonic buffer (4 mL) containing APA (200 μg/mL), reduced glutathione (GSH) (3×10^{-3} M), ATP (2×10^{-3} M) and some other stabilizer was gradually mixed with RBC suspension (1 mL) then the mixture was put into 4 °C for about 40 min. After centrifugation, the sediment was resealed in a hypertonic solution at 37 °C for 40 min. The redundant APA was discarded by PBS washing.

Characterization of A@RBC. After hypotonic process, the UV−vis spectra and mass spectrum were carried out to conform the successful preparation of A@RBC. The A@RBC sample was disintegrated by RBC lysis buffer, and the whole APA was purified by centrifugation and filtration of 200 nm strainer. The loaded content of APA was determined by UV−vis spectra. The morphology of original RBC, A@RBC, A@RBC + EF, and A@RBC after EF was observed by optical microscope and scan electron microscopy (SEM) after gradient centrifugation.

Preparation of the Flexible Interdigital Electrode. The positive photoresist was spinning coated on a PET film (2000 rpm, 30 s) then heated at 75 °C for 2 min. After that the dry photoresist was exposed by ultraviolet light for 15s. After exposure, the PET film was baked at 75 °C for 2 min and soaked in the photoresist developer to form interdigital model. A Cu membrane was magnetron sputtered on the surface of the interdigital model. Then the PET film was soaked in stripping chemicals for positive resist, forming the flexible interdigital electrodes. An ultrathin PDMS membrane was deposited on the surface of the electrodes for encapsulation as well as insulation.

In Vitro Cell Experiment. The hepa1−6 cells were cultured in DMEM medium containing 10% (v/v) fetal bovine serum (FBS), streptomycin (100 g mL^{-1}) and penicillin (100 U mL^{-1}). After the hepa1−6 cells were seeded and cultured for 12 h, they were divided into eight groups including control, EF, RBC, RBC+EF, APA, APA +EF, A@RBC and A@RBC+EF. Every group contained at least triplicate parallel tests.

***In Vivo* Subcutaneous Liver Tumor of Mouse.** The experimental c57 mice (female, 4−5 weeks old) were feeded in the lab for 1 week, the hepal-6 tumor cells were implanted in the subcutaneous part of hind leg. Six $\times 10^6$ hepa1−6 cells in 100 μL PBS were injected subcutaneously into the right side of the mice to form liver tumors. After tumor volumes reached about 100 mm^3, various treatments were carried out.

***In Vivo* Tumor Accumulation of A@RBC.** The membrane of A@RBC was stained by red fluorescent dye (DiD). After ultrasonic treatment, the A@RBC was inoculated to hepal-6 tumor-bearing mice through tail vein with the APA dose of 5 mg/kg body weight. At 12 h, 24 h, 48 h, and 96 h, respectively, the distribution images of A@RBC were obtained by the *in vivo* animal imaging system.

***In Vivo* Antitumor Evaluation of Mouse.** Commercial medical steel microneedles were utilized for delivering EF generated by the iTENG. The tip parts of the microneedles were deposited by perylene for insulation. Sixty c57 black mice were randomly separated into control, APA, APA+EF, A@RBC, and A@RBC+EF groups. 200 μL PBS, APA, or A@RBC were intravenously administrated to different groups with the APA dose of 5 mg/kg body weight. Three drug administrations on Day 7, Day 9, and Day11 were carried out. Judged by *in vivo* accumulation of A@RBC, the iTENGs worked about 12 h after the drug injection for 20 min each time. The microneedle electrodes connected to the iTENG were parallelly inserted into the tumors. The tumor volume was recorded every 2 days. On Day 28, half the mice in each group were euthanized. The tumor size and morphology were obtained using a digital camera. Besides, HE and anti-Ki67 immunohistochemical assay was obtained with the tumor slices. The remaining mice were used for recording the survival time.

***In Vivo* Antitumor Evaluation of Rabbit.** Twenty-five rabbits were inoculated with VX2 cells in the liver. After the tumors grow to about 1 cm in diameter, the tumor bearing rabbits were randomly separated into control (PBS), APA, APA+EF, A@RBC, and A@RBC +EF groups. The PBS, APA, or A@RBC with the APA dose of 5 mg/kg body weight was injected to rabbits through marginal ear vein respectively on Day 1, Day 3, Day 5, and Day 7. The iTENG and soft electrode membrane were stacked tightly and put between the liver and diaphragm, and microneedle electrodes were inserted into the tumor. EF stimulation was generated by respiration action. The angiography images were obtained under digital subtraction angiography (DSA). Besides, the enhanced computed tomography

https://doi.org/10.1021/acsnano.2c03768
ACS Nano XXXX, XXX, XXX−XXX

(CT) was performed on Day 7 and Day 21 and then one tumor bearing rabbit of each group was sacrificed to obtain the specimens. HE stain assay and CD31 immunohistochemical staining experiment were done with the tumor paraffin slices. The animal experiments were approved by the Institutional Animal Care and Use Committee at Tongji Medical College, Huazhong University of Science and Technology (IACUC-S2525).

ASSOCIATED CONTENT

Supporting Information

The Supporting Information is available free of charge at https://pubs.acs.org/doi/10.1021/acsnano.2c03768.

Transferred charges of iTENGs with circle, rectangle, square, and rhombus shape; influence of pH on the hypotonic process; mass spectra of APA and RBC; calibration curve of APA absorbance versus its concentrations; effect of voltage on the APA release from A@RBC; APA release curve when simulated continuously for 24 h at 32 V; SEM image of A@RBC after stimulation for 3 days with the voltage of 180 V; fluorescence images of all major organs when compared to the tumors for the control and treated animals at 72 h; image of the harvested tumors in each group; Ki67 immunohistochemistry images of the tumors in various groups (scale bar: 200 μm); body weight of mice in each group; HE and Masson's trichrome staining on the tissue formed around the implants retrieved at 1, 2, and 3 months; flow cytometry of host innate immune macrophages; flow cytometry of host innate immune neutrophils; voltage outputs of the iTENGs implanted for 1, 2, and 3 months; iTENG based devices implanted between the tumor and diaphragm to provide EF; voltage output of the iTENG after implanted in the rabbits; enhanced CT scan (the upside, scale bar: 1 cm) and digital image (the downside) of tumors in each group on Day 7; Ki67 immunohistochemistry images of the tumors in various group (scale bar: 200 μm) (PDF)

AUTHOR INFORMATION

Corresponding Authors

Bin Xiong − *Department of Radiology, Union Hospital, Tongji Medical College, Huazhong University of Science and Technology, Wuhan 430022, China;* orcid.org/0000-0002-7795-7041; Email: herr_xiong@126.com

Zhou Li − *CAS Center for Excellence in Nanoscience, Beijing Key Laboratory of Micro-nano Energy and Sensor, Beijing Institute of Nanoenergy and Nanosystems, Chinese Academy of Sciences, Beijing 101400, China; School of Nanoscience and Technology, University of Chinese Academy of Sciences, Beijing 100049, China; Center on Nanoenergy Research, School of Physical Science and Technology, Guangxi University, Nanning 530004, China;* orcid.org/0000-0002-9952-7296; Email: zli@binn.cas.cn

Authors

Chaochao Zhao − *Department of Biomedical Engineering, School of Medicine, Foshan University, Foshan 528225, China; CAS Center for Excellence in Nanoscience, Beijing Key Laboratory of Micro-nano Energy and Sensor, Beijing Institute of Nanoenergy and Nanosystems, Chinese Academy of Sciences, Beijing 101400, China;* orcid.org/0000-0002-6698-241X

Qin Shi − *Department of Radiology, Union Hospital, Tongji Medical College, Huazhong University of Science and Technology, Wuhan 430022, China; Department of Interventional Radiology, Zhongshan Hospital, Fudan University, Shanghai 200032, China*

Hu Li − *CAS Center for Excellence in Nanoscience, Beijing Key Laboratory of Micro-nano Energy and Sensor, Beijing Institute of Nanoenergy and Nanosystems, Chinese Academy of Sciences, Beijing 101400, China*

Xi Cui − *CAS Center for Excellence in Nanoscience, Beijing Key Laboratory of Micro-nano Energy and Sensor, Beijing Institute of Nanoenergy and Nanosystems, Chinese Academy of Sciences, Beijing 101400, China; School of Nanoscience and Technology, University of Chinese Academy of Sciences, Beijing 100049, China*

Yuan Xi − *CAS Center for Excellence in Nanoscience, Beijing Key Laboratory of Micro-nano Energy and Sensor, Beijing Institute of Nanoenergy and Nanosystems, Chinese Academy of Sciences, Beijing 101400, China*

Yu Cao − *CAS Center for Excellence in Nanoscience, Beijing Key Laboratory of Micro-nano Energy and Sensor, Beijing Institute of Nanoenergy and Nanosystems, Chinese Academy of Sciences, Beijing 101400, China; Center on Nanoenergy Research, School of Physical Science and Technology, Guangxi University, Nanning 530004, China*

Zhuo Xiang − *CAS Center for Excellence in Nanoscience, Beijing Key Laboratory of Micro-nano Energy and Sensor, Beijing Institute of Nanoenergy and Nanosystems, Chinese Academy of Sciences, Beijing 101400, China; Center on Nanoenergy Research, School of Physical Science and Technology, Guangxi University, Nanning 530004, China*

Feng Li − *State Key Laboratory of Biochemical Engineering, Institute of Process Engineering, Chinese Academy of Sciences, Beijing 100190, China*

Jinyan Sun − *Department of Biomedical Engineering, School of Medicine, Foshan University, Foshan 528225, China*

Jiacheng Liu − *Department of Radiology, Union Hospital, Tongji Medical College, Huazhong University of Science and Technology, Wuhan 430022, China;* orcid.org/0000-0002-7786-9957

Tongqiang Li − *Department of Radiology, Union Hospital, Tongji Medical College, Huazhong University of Science and Technology, Wuhan 430022, China*

Wei Wei − *State Key Laboratory of Biochemical Engineering, Institute of Process Engineering, Chinese Academy of Sciences, Beijing 100190, China;* orcid.org/0000-0002-6244-3187

Complete contact information is available at: https://pubs.acs.org/10.1021/acsnano.2c03768

Author Contributions

The manuscript was written through contributions of all authors. All authors have given approval to the final version of the manuscript. Z.L. and B.X. guided the project, conceived the idea, and designed the experiment. W.W. guided the mouse experiment. C.Z., Q.S., and H.L. made the experiment, improved the scheme, and developed the writing plan. X.C., Q.S., J.L., and T.L. carried out the rabbit experiment and collected data. X.C., Y.C., and C.Z. made the mouse experiment. C.Z. and Z.X. carried out the cell experiment. F.L. carried out the animal imaging work. C.Z., Y.X., and J.S. drew the figures and revised the manuscript. All authors

https://doi.org/10.1021/acsnano.2c03768
ACS Nano XXXX, XXX, XXX−XXX

discussed and reviewed the manuscript. C.Z., Q.S., and H.L. contributed equally.

Notes

The authors declare no competing financial interest.

ACKNOWLEDGMENTS

This work was supported by National Natural Science Foundation of China (T2125003, 61875015, 82001981, 81873917), Foshan Bureau of Finance: Developmental and Applied Basic Research of Advanced Technology in Stomatology (CGQ020), the Guangdong Basic and Applied Basic Research Foundation (2019A1515110639), the Scientific Research Foundation for Advanced Scholars of Foshan University (Gg07247, Gg07164), and the Beijing Natural Science Foundation (JQ20038).

REFERENCES

(1) Sia, D.; Villanueva, A.; Friedman, S. L.; Llovet, J. M. Liver Cancer Cell of Origin, Molecular Class, and Effects on Patient Prognosis. *Gastroenterology* **2017**, *152*, 745−761.

(2) Parayath, N. N.; Stephan, S. B.; Koehne, A. L.; Nelson, P. S.; Stephan, M. T. In vitro-transcribed antigen receptor mRNA nanocarriers for transient expression in circulating T cells in vivo. *Nat. Commun.* **2020**, *11*, 6080.

(3) Zhou, T. J.; Liang, X. L.; Wang, P. F.; Hu, Y. Y.; Qi, Y. F.; Jin, Y. S.; Du, Y.; Fang, C. H.; Tian, J. A Hepatocellular Carcinoma Targeting Nanostrategy with Hypoxia-Ameliorating and Photothermal Abilities that, Combined with Immunotherapy, Inhibits Metastasis and Recurrence. *ACS Nano* **2020**, *14*, 12679−12696.

(4) Kariyama, K.; Nouso, K.; Hiraoka, A.; Wakuta, A.; Oonishi, A.; Kuzuya, T.; Toyoda, H.; Tada, T.; Tsuji, K.; Itobayashi, E.; Ishikawa, T.; Takaguchi, K.; Tsutsui, A.; Shimada, N.; Kudo, M.; Kumada, T. EZ-ALBI Score for Predicting Hepatocellular Carcinoma Prognosis. *Liver Cancer* **2020**, *9*, 734−743.

(5) Marasco, G.; Serenari, M.; Renzulli, M.; Alemanni, L. V.; Rossini, B.; Pettinari, I.; Dajti, E.; Ravaioli, F.; Golfieri, R.; Cescon, M.; Festi, D.; Colecchia, A. Clinical impact of sarcopenia assessment in patients with hepatocellular carcinoma undergoing treatments. *J. Gastroenterol* **2020**, *55*, 927−943.

(6) Jang, W. I.; Bae, S. H.; Kim, M. S.; Han, C. J.; Park, S. C.; Kim, S. B.; Cho, E. H.; Choi, C. W.; Kim, K. S.; Hwang, S.; Kim, J. H.; Chang, A. R.; Park, Y.; Kim, E. S.; Kim, W. C.; Jo, S.; Park, H. J. A phase 2 multicenter study of stereotactic body radiotherapy for hepatocellular carcinoma: Safety and efficacy. *Cancer* **2020**, *126*, 363−372.

(7) Manghnani, P. N.; Wu, W. B.; Xu, S. D.; Hu, F.; Teh, C.; Liu, B. Visualizing Photodynamic Therapy in Transgenic Zebrafish Using Organic Nanoparticles with Aggregation-Induced Emission. *Nano-Micro Lett.* **2018**, *10*, 61.

(8) Hwang, L.; Paluch, J.; Jadvar, H.; England, J. R.; Desai, B.; Ballas, L. K. Salvage Therapies After F-18-Fluciclovine Detected Prostate Cancer Recurrences. *Clin. Nucl. Med.* **2020**, *45*, 668−671.

(9) Sebastian, N. T.; Miller, E. D.; Yang, X.; Diaz, D. A.; Tan, Y.; Dowell, J.; Spain, J.; Rikabi, A.; Elliott, E.; Knopp, M.; Williams, T. M. A Pilot Trial Evaluating Stereotactic Body Radiation Therapy to Induce Hyperemia in Combination With Transarterial Chemoembolization for Hepatocellular Carcinoma. *Int. J. Radiat. Oncol. Biol. Phys.* **2020**, *108*, 1276−1283.

(10) Zhang, C. Y.; Wang, X.; Du, J. F.; Gu, Z. J.; Zhao, Y. L. Reactive Oxygen Species-Regulating Strategies Based on Nanomaterials for Disease Treatment. *Adv. Sci.* **2021**, *8*, 2002797.

(11) Hao, H. S.; Chen, Y.; Wu, M. Y. Biomimetic nanomedicine toward personalized disease theranostics. *Nano Res.* **2021**, *14*, 2941−2511.

(12) Yin, H. H.; Zhou, B. G.; Zhao, C. K.; Sun, L. P.; Yue, W. W.; Li, X. L.; Li, H. Y.; Li, S. Y.; Xu, H. X.; Chen, Y. 2D Core/Shell-Structured Mesoporous Silicene@Silica for Targeted and Synergistic NIR-II-Induced Photothermal Ablation and Hypoxia-Activated Chemotherapy of Tumor. *Adv. Funct. Mater.* **2021**, *31*, 2102043.

(13) Wu, Y. Z.; Chen, F. M.; Huang, N. W.; Li, J. J.; Wu, C. Z.; Tan, B. W.; Liu, Y. K.; Li, L. J.; Yang, C.; Shao, D.; Liao, J. F. Near-infrared light-responsive hybrid hydrogels for the synergistic chemo-photothermal therapy of oral cancer. *Nanoscale* **2021**, *13*, 17168−17182.

(14) Conde, J.; Pumroy, R. A.; Baker, C.; Rodrigues, T.; Guerreiro, A.; Sousa, B. B.; Marques, M. C.; de Almeida, B. P.; Lee, S.; Leites, E. P.; Picard, D.; Samanta, A.; Vaz, S. H.; Sieglitz, F.; Langini, M.; Remke, M.; Roque, R.; Weiss, T.; Weller, M.; Liu, Y. H.; Han, S.; Corzana, F.; Morais, V. A.; Faria, C. C.; Carvalho, T.; Filippakopoulos, P.; Snijder, B.; Barbosa-Morais, N. L.; Moiseenkova-Bell, V. Y.; Bernardes, G. J. L. Allosteric Antagonist Modulation of TRPV2 by Piperlongumine Impairs Glioblastoma Progression. *Acs Central Sci.* **2021**, *7*, 868−881.

(15) Yang, X.; Gao, L.; Wei, Y. F.; Tan, B. W.; Wu, Y. Z.; Yi, C.; Liao, J. F. Photothermal hydrogel platform for prevention of post-surgical tumor recurrence and improving breast reconstruction. *J. Nanobiotechnol.* **2021**, *19*, 307−319.

(16) Gilam, A.; Conde, J.; Weissglas-Volkov, D.; Oliva, N.; Friedman, E.; Artzi, N.; Shomron, N. Local microRNA delivery targets Palladin and prevents metastatic breast cancer. *Nat. Commun.* **2016**, *7*, 12868.

(17) Conde, J.; Oliva, N.; Artzi, N. Implantable hydrogel embedded dark-gold nanoswitch as a theranostic probe to sense and overcome cancer multidrug resistance. *P. Natl. Acad. Sci. USA* **2015**, *112*, E1278−E1287.

(18) Conde, J.; Oliva, N.; Zhang, Y.; Artzi, N. Local triple-combination therapy results in tumour regression and prevents recurrence in a colon cancer model. *Nat. Mater.* **2016**, *15*, 1128−1138.

(19) Conde, J.; Oliva, N.; Atilano, M.; Song, H. S.; Artzi, N. Self-assembled RNA-triple-helix hydrogel scaffold for microRNA modulation in the tumour microenvironment. *Nat. Mater.* **2016**, *15*, 353−363.

(20) Timin, A. S.; Litvak, M. M.; Gorin, D. A.; Atochina-Vasserman, E. N.; Atochin, D. N.; Sukhorukov, G. B. Cell-Based Drug Delivery and Use of Nano- and Microcarriers for Cell Functionalization. *Adv. Healthc. Mater.* **2018**, *7*, 1870012.

(21) Pierige, F.; Serafini, S.; Rossi, L.; Magnani, A. Cell-based drug delivery. *Adv. Drug Deliver. Rev.* **2008**, *60*, 286−295.

(22) Chu, L.; Chen, Y.; Liu, Q.; Liang, F.; Wang, S.; Liu, Q.; Yu, H.; Wu, X.; Zhang, J.; Deng, J.; Ai, D.; Zhu, Z.; Nie, Y.; Zhao, K. A Phase II Study of Apatinib in Patients with Chemotherapy-Refractory Esophageal Squamous Cell Carcinoma (ESO-Shanghai 11). *Oncologist* **2021**, *26*, e925−e935.

(23) Vazquez, R.; Riveiro, M. E.; Berenguer-Daize, C.; O'Kane, A.; Gormley, J.; Touzelet, O.; Rezai, K.; Bekradda, M.; Ouafik, L. Targeting Adrenomedullin in Oncology: A Feasible Strategy With Potential as Much More Than an Alternative Anti-Angiogenic Therapy. *Front Oncol* **2021**, *10*, 589218.

(24) Jia, X. Q.; Wen, Z. P.; Sun, Q. Y.; Zhao, X. H.; Yang, H.; Shi, X. Y.; Xin, T. Apatinib suppresses the proliferation and apoptosis of gastric cancer cells via the PI3K/Akt signaling pathway. *J. Buon.* **2019**, *24*, 1985−1991.

(25) Zhang, H.; Cao, Y. M.; Chen, Y. R.; Li, G. X.; Yu, H. S. Apatinib promotes apoptosis of the SMMC-7721 hepatocellular carcinoma cell line via the PI3K/Akt pathway. *Oncol. Lett.* **2018**, *15*, 5739−5743.

(26) Kinosita, K., Jr.; Tsong, T. Y. Formation and resealing of pores of controlled sizes in human erythrocyte membrane. *Nature* **1977**, *268*, 438−41.

(27) Rao, L.; Cai, B.; Bu, L. L.; Liao, Q. Q.; Guo, S. S.; Zhao, X. Z.; Dong, W. F.; Liu, W. Microfluidic Electroporation-Facilitated Synthesis of Erythrocyte Membrane-Coated Magnetic Nanoparticles for Enhanced Imaging-Guided Cancer Therapy. *ACS Nano* **2017**, *11*, 3496−3505.

https://doi.org/10.1021/acsnano.2c03768
ACS Nano XXXX, XXX, XXX−XXX

(28) Zhao, C. C.; Cui, X.; Wu, Y. X.; Li, Z. Recent Progress of Nanogenerators Acting as Self-Powered Drug Delivery Devices. *Adv. Sustain. Syst.* **2021**, *5*, 2000268.
(29) Feng, H. Q.; Zhao, C. C.; Tan, P. C.; Liu, R. P.; Chen, X.; Li, Z. Nanogenerator for Biomedical Applications. *Adv. Healthc. Mater.* **2018**, *7*, 1701298.
(30) Liu, Z.; Ma, Y.; Ouyang, H.; Shi, B. J.; Li, N.; Jiang, D. J.; Xie, F.; Qu, D.; Zou, Y.; Huang, Y.; Li, H.; Zhao, C. C.; Tan, P. C.; Yu, M.; Fan, Y. B.; Zhang, H.; Wang, Z. L.; Li, Z. Transcatheter Self-Powered Ultrasensitive Endocardial Pressure Sensor. *Adv. Funct. Mater.* **2019**, *29*, 1807560.
(31) Sun, J. Y.; Yang, A. P.; Zhao, C. C.; Liu, F.; Li, Z. Recent progress of nanogenerators acting as biomedical sensors in vivo. *Sci. Bull.* **2019**, *64*, 1336−1347.
(32) Jiang, W.; Li, H.; Liu, Z.; Li, Z.; Tian, J. J.; Shi, B. J.; Zou, Y.; Ouyang, H.; Zhao, C. C.; Zhao, L. M.; Sun, R.; Zheng, H. R.; Fan, Y. B.; Wang, Z. L.; Li, Z. Fully Bioabsorbable Natural-Materials-Based Triboelectric Nanogenerators. *Adv. Mater.* **2018**, *30*, 1801895.
(33) Shi, R.; Zhang, J. S.; Tian, J. J.; Zhao, C. C.; Li, Z.; Zhang, Y. Z.; Li, Y. S.; Wu, C. G.; Tian, W.; Li, Z. An effective self-powered strategy to endow titanium implant surface with associated activity of anti-biofilm and osteogenesis. *Nano Energy* **2020**, *77*, 105201.
(34) Zou, Y.; Liao, J. W.; Ouyang, H.; Jiang, D. J.; Zhao, C. C.; Li, Z.; Qu, X. C.; Liu, Z.; Fan, Y. B.; Shi, B. J.; Zheng, L.; Li, Z. A flexible self-arched biosensor based on combination of piezoelectric and triboelectric effects. *Appl. Mater. Today* **2020**, *20*, 100699.
(35) Zhao, C. C.; Feng, H. Q.; Zhang, L. J.; Li, Z.; Zou, Y.; Tan, P. C.; Ouyang, H.; Jiang, D. J.; Yu, M.; Wang, C.; Li, H.; Xu, L. L.; Wei, W.; Li, Z. Highly Efficient In Vivo Cancer Therapy by an Implantable Magnet Triboelectric Nanogenerator. *Adv. Funct. Mater.* **2019**, *29*, 1808640.
(36) Liu, Z.; Li, H.; Shi, B. J.; Fan, Y. B.; Wang, Z. L.; Li, Z. Wearable and Implantable Triboelectric Nanogenerators. *Adv. Funct. Mater.* **2019**, *29*, 1808820.
(37) Yao, W. T.; Wu, F. X.; Cai, Q. Q.; Wang, J. Q. Efficacy and safety of apatinib in advanced sarcoma: an open-label, non-randomized, single-center study of 45 patients. *Anti-Cancer Drug* **2019**, *30*, 749−756.
(38) Meng, M.; Ye, X.; Yang, X.; Huang, G. H.; Wei, Z. G.; Ni, Y.; Li, W. H.; Han, X. Y.; Wang, J. Apatinib and S-1 combination therapy for the treatment of advanced head and neck neoplasms: Three case reports. *J. Cancer Res. Ther.* **2019**, *15*, 442−446.
(39) Cheng, H. Y.; Zong, L. J.; Kong, Y. J.; Wang, X. Y.; Gu, Y.; Cang, W.; Zhao, J.; Wan, X. R.; Yang, J. J.; Xiang, Y. Camrelizumab plus apatinib in patients with high-risk chemorefractory or relapsed gestational trophoblastic neoplasia (CAP 01): a single-arm, open-label, phase 2 trial. *Lancet Oncol* **2021**, *22*, 1609−1617.
(40) Liu, Z. J.; Wang, C. M.; Wu, G. Y.; Cheng, J. Y. MRI analysis of hydrogel-loaded apatinib for local therapy of hepatocellular carcinoma model in nude mice. *Biochem. Bioph. Res. Co.* **2019**, *509*, 529−534.
(41) He, Y.; Li, X.; Ma, J.; Ni, G.; Yang, G.; Zhou, S. Programmable Codelivery of Doxorubicin and Apatinib Using an Implantable Hierarchical-Structured Fiber Device for Overcoming Cancer Multi-drug Resistance. *Small* **2019**, *15*, No. e1804397.
(42) Wang, Y. L.; Tang, Z. G. A novel long-sustaining system of apatinib for long-term inhibition of the proliferation of hepatocellular carcinoma cells. *Oncotargets Ther* **2018**, *11*, 8529−8541.
(43) Yu, T.; Wu, C.; Zhu, C. H.; He, Y. H.; Yang, D. K.; Cheng, Y. Z.; Gao, X. Oral Administration of Liposome-Apatinib and Locally Delivery of Docetaxel/MPEG-PCL by Fibrin Glue Synergistically Improve Therapeutic Effect in Colorectal Cancer. *J. Biomed. Nanotechnol.* **2018**, *14*, 2077−2091.
(44) Min, H.; Wang, J.; Qi, Y. Q.; Zhang, Y. L.; Han, X. X.; Xu, Y.; Xu, J. C.; Li, Y.; Chen, L.; Cheng, K. M.; Liu, G. N.; Yang, N.; Li, Y. Y.; Nie, G. J. Biomimetic Metal-Organic Framework Nanoparticles for Cooperative Combination of Antiangiogenesis and Photodynamic Therapy for Enhanced Efficacy. *Adv. Mater.* **2019**, *31*, 1808200.
(45) Dai, Y. X.; Wang, S.; Shi, W. B.; Lang, M. D. pH-responsive carboxymethyl chitosan-derived micelles as apatinib carriers for effective anti-angiogenesis activity: Preparation and in vitro evaluation. *Carbohyd. Polym.* **2017**, *176*, 107−116.
(46) Zhao, C. C.; Yang, Y.; Cui, X.; Shan, Y. Z.; Xue, J. T.; Jiang, D. J.; Sun, J. Y.; Li, N.; Li, Z.; Yang, A. P. Self-Powered Electrical Impulse Chemotherapy for Oral Squamous Cell Carcinoma. *Materials* **2022**, *15*, 2060.

https://doi.org/10.1021/acsnano.2c03768
ACS Nano XXXX, XXX, XXX−XXX